THE JOURNAL OF PHYSICAL CHEMISTRY LETTERS
A JOURNAL OF THE AMERICAN CHEMICAL SOCIETY

pubs.acs.org/JPCL

Letter

Electric-Field-Driven Ion Emission from the Free Surface of Room Temperature Ionic Liquids

Fei Zhang, Xikai Jiang,* Gaofeng Chen, Yadong He, Guoqing Hu, and Rui Qiao

Cite This: J. Phys. Chem. Lett. 2021, 12, 711−716

Read Online

ACCESS | Metrics & More | Article Recommendations

ABSTRACT: Electric-field-driven ion emission from the free surface of a planar room-temperature ionic liquid (RTIL) film was studied by using molecular dynamics simulations. We calculated ion emission rate (j_e) as a function of the electric field normal to the RTIL/vacuum surface (E_n) and found that the logarithm of j_e over the charge density on the surface (σ) is proportional to $E_n^{1/2}$, in agreement with classical ion evaporation theories. The composition of emitted ions includes monomers and dimers. It was found that the monomer has to move across two barriers before emission. The fraction of dimers was found to depend on the external field and ion−ion interactions. We further performed replica exchange molecular dynamics simulations and identified different metastable states of the emitting ion near the liquid film. Our results showed that E_n and molecular details of ion/surface determine the rate and composition of ion emission from RTIL/vacuum surfaces. Fundamental insights revealed in this study form the basis to improve ion evaporation theories and performance of electrospray applications ranging from space propulsion to nanomanufacturing.

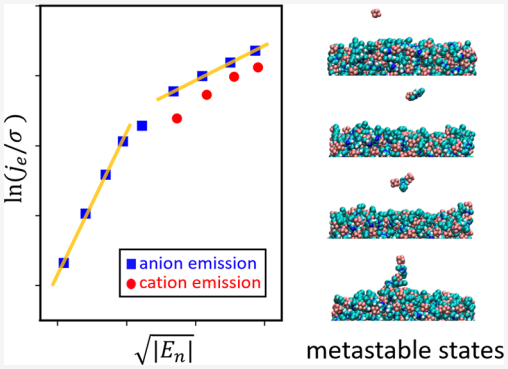

Under external electric fields, various species such as ions/droplets may emit from electrically conducting liquids.[1−3] This phenomenon is often termed electrospray, which has applications ranging from mass spectrometry to space propulsion.[4−7] The operation of electrospray is classified into three modes: purely ionic mode, purely droplet mode, and mixed droplet−ion mode.[1] Past research focused primarily on electrosprays in the droplet mode because of their importance in technologies such as mass spectrometry.[3−6] Few studies focused on the electrospray in purely ionic mode because such an operation is difficult to achieve with volatile nonmetallic liquids.[8,9] The situation was changed when ionic liquid ion sources (ILIS) were introduced.[10] ILIS were demonstrated to operate in the purely ionic mode and generate ion beams with high charge/mass ratio and diverse ion species, which make them promising in fields such as space propulsion and nanomanufacturing.[7] Room temperature ionic liquids (RTILs) were used in ILIS, and they are made solely of ions but are liquid at room temperature.[11] RTILs have low vapor pressure, and their properties can be tailored by numerous combinations of cations and anions, which make them useful in electrosprays. To theoretically describe ion emission in electrosprays, an ion evaporation model was developed in which ions evaporate from liquid/vacuum surfaces, and the ion emission rate is[12−14]

$$j_e = \frac{k_B T}{h}\sigma \exp\left(-\frac{\Delta G - G(E_n)}{k_B T}\right) \quad (1)$$

where k_B is Boltzmann's constant, T is the liquid temperature, h is Planck's constant, σ is the net charge density on the liquid/vacuum surface, ΔG is the Gibbs free energy of solvation of an emitted ion/cluster, and E_n is the electric field normal to the surface. $G(E_n) = \sqrt{\frac{q^3 E_n}{4\pi\epsilon_0}\frac{\epsilon_r - 1}{\epsilon_r + 1}}$ is the reduction to ΔG by the Schottky hump, where q is the ion's charge, ϵ_0 is the vacuum permittivity, and ϵ_r is the dielectric constant of the liquid. According to the Born model, the solvation energy of the emitted ion/cluster of charge q is $\Delta G = (27\pi/4)^{1/3}\frac{\gamma^{1/3} q^{4/3}(1-\epsilon_r^{-1})^{2/3}}{(4\pi\epsilon_0)^{2/3}}$, where γ is the surface tension of the liquid.[13] If γ/ϵ_r of the liquid increases (decreases) as the applied electric field increases, ΔG will increase (decrease). Ion emission from liquid/vacuum surfaces is governed by the free energy landscape for ions moving across the surface into a vacuum. The predicted energy barrier's peak is at a distance $x^* = \sqrt{\frac{q}{16\pi\epsilon_0 E_n}\frac{\epsilon_r - 1}{\epsilon_r + 1}}$ away from the surface.[12,13,15]

Received: November 7, 2020
Accepted: December 29, 2020
Published: January 5, 2021

Despite significant progress,[16,17] issues on critical aspects of purely ionic electrosprays of RTILs remain to be resolved. In existing ion evaporation theories, ions differ from each other only in their bulk solvation energy; no molecular details of surface/ion are considered: the liquid/vacuum surface is flat, and ions are point charges. However, RTIL/vacuum surfaces typically have a roughness of 3 Å,[18] and the ions are often bulky (e.g., an $[EMI^+]$ is ∼8 Å long). Therefore, an ion at positions up to the energy barrier's peak (often ∼4−5 Å from the surface) is likely in contact with the surface and modifies the surface locally. Furthermore, reported purely ionic emissions feature a large fraction of dimers and some trimers, a fact not considered in original theories.[10,15,19] The predicting power of ion evaporation theories is thus limited in these conditions. The above issues can in principle be addressed by using molecular dynamics (MD) simulations. However, available simulations focused on ion emission from complex systems such as molecular droplets/cones,[1,20−22] in which complex processes (e.g., generation of molecularly sharp meniscus) make it difficult to quantitatively address the issues and mechanistically understand ion emission characteristics. In addition, to the best of our knowledge, eq 1 in ion evaporation theories has not been verified by MD simulations. Here, we seek to address the issues by studying ion emissions from the free surface of a planar RTIL film using MD simulations.

Figure 1 shows a schematic of the MD simulation system and the coarse-grained and united atom models for 1-butyl-3-

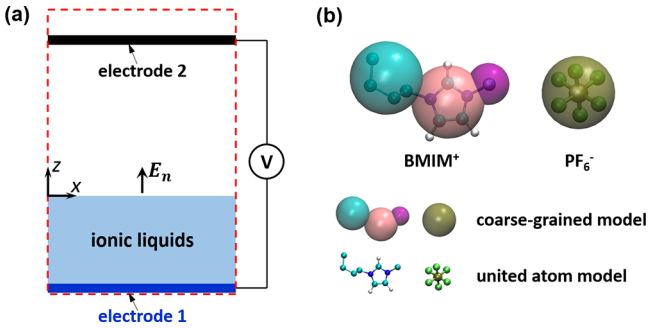

Figure 1. (a) Schematic of the MD simulation system. The dashed lines denote the simulation box. (b) Two models of $[BMIM][PF_6]$ used in MD simulations.

methylimidazolium hexafluorophosphate ($[BMIM][PF_6]$). The simulation system in Figure 1a contains two planar electrodes that are made of carbon atoms. $[BMIM][PF_6]$ molecules are placed near the lower electrode to mimic a planar film subject to external electric fields. The film's thickness is ∼7 nm to eliminate the influence of the electrical double layer near the lower electrode on ion emission. The simulation box measures $7 \times 7 \times 50$ nm^3 ($x \times y \times z$). We define $z = 0$ nm to be the dividing surface (RTIL/vacuum surface) position, where the mass density of the RTIL is half of its bulk value. All the heights (z) in this paper are with respect to this dividing surface. A planar film is used because: (1) For purely ionic electrosprays, the radius of curvature of the liquid meniscus' tip is ∼5−10 nm for typical RTILs.[10,23] Because this radius is much larger than the size of emitted ions, we can neglect the mesoscopic curvature of the RTIL/vacuum surface. (2) Adopting a planar film makes it straightforward to measure and control E_n. It eliminates uncertainties in surface electric fields of small cones/droplets, where E_n varies spatially and temporally on the RTIL/vacuum surface.[20,21] Figure 1b shows coarse-grained and united atom models for $[BMIM][PF_6]$. Both models were parametrized to reproduce experimentally measured properties such as density, self-diffusion coefficient, and viscosity.[24,25] The coarse-grained model greatly reduces the computational cost and is valuable for studying phenomena that occur on a larger length/time scale; the united atom model can provide more atomistic details on ion emission.

To drive the ion emission, an electrical potential difference is applied between two electrodes by using a special electrostatic method.[26] We have implemented this method into Gromacs[27] and used it to study charge storages in nanopores successfully.[28] The potential on the lower electrode ($z = -6.3$ nm) is 0 V, and the potential on the upper electrode ($z = 38.7$ nm) varies from ±40 to ±100 V to generate different E_n. The positive directions of E_n and force of the emitting ion are in the positive z-direction. Because an accurate evaluation of j_e is computationally expensive when E_n is very weak, we use the coarse-grained model to calculate j_e. Simulations are performed in the NVT ensemble ($T = 400$ K). A Berendsen thermostat with a time constant of 0.2 ps is used. The electrostatic interaction is computed by using the particle mesh Ewald (PME) method with a real-space cutoff radius of 1.5 nm and an FFT spacing of 0.13 nm. Nonelectrostatic interactions are computed with a cutoff radius of 1.5 nm. The time step is 2 fs, and the neighbor list is updated every step. The film is packed into the system by using Packmol[29] and then equilibrated for 500 ps, which is followed by a 400 ps production run. As translational diffusion coefficients of ions are $\sim 200 \times 10^{-12}$ m^2/s at 400 K,[25] ions diffuse ∼0.3 nm after 500 ps, which is enough for the system to reach equilibrium from the initial configuration where RTIL molecules are uniformly distributed. For $E_n \leqslant 1.7$ V/nm and $E_n > 1.7$ V/nm, 100 and 10 independent simulations are performed respectively. In each simulation, ion emission events are monitored on the fly. An ion emission event is registered when an ion or ion cluster reaches a detection plane that is located at a distance of ∼10 nm above the RTIL/vacuum surface. The ion emission rate is calculated by dividing the total amount of charges across the detection plane in a production run by the area of the detection plane (49 nm^2) and the total simulation time. When an ion (or each ion in an ion cluster) moves to a position that is less than 1 nm away from the upper electrode, it is moved to a position above the upper electrode and fixed there afterward. This method ensures the MD system's electroneutrality, as required by the PME method. Ions fixed above the upper electrode are electrostatically invisible to the ions between the lower and upper electrodes as they are in the Faraday cage formed by the upper electrode and the periodical image of the lower electrode.[28] The charge density on the RTIL/vacuum surface is $\sigma = \epsilon_0(E_n^v - E_n^l)$.[3] The normal electric fields at the surface on the vacuum side (E_n^v) and liquid side (E_n^l) are calculated from electrical potential profile $\phi(z)$ and are averaged among independent simulations. $\phi(z)$ is calculated by using methods in ref 30.

Parameters in simulations with the united atom model are the same as those in coarse-grained simulations, except that constant electric field is applied after the equilibration run. These simulations are stopped after the first ion emission event, and we obtain 100 ion emission events for each case by running 100 independent simulations. Furthermore, replica exchange molecular dynamics (REMD) simulations[31] are performed to examine metastable states of the emitted ion,

https://dx.doi.org/10.1021/acs.jpclett.0c03335
J. Phys. Chem. Lett. 2021, 12, 711−716

in which we constrain one anion at z = 1.9 nm and apply a field of 0.9 V/nm. We use this field because it does not trigger ion emission, as the emission could complicate the analysis on metastable states. Twenty replicas are used with temperatures evenly distributed from 400 to 495 K. Exchange rates between two adjacent replicas are verified to be ∼20%. We perform REMD for 8 ns and record forces and configurations every 20 fs.

Figure 2 shows the $\ln(j_e/\sigma)-E_n^{1/2}$ relationship. Anion emission rates from MD simulations can be fitted to the ion

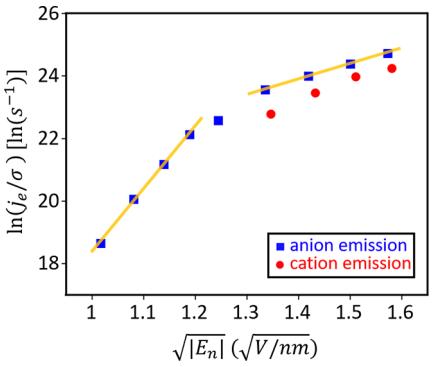

Figure 2. Logarithm of the ion emission rate over the charge density on the RTIL/vacuum surface, $\ln(j_e/\sigma)$, as a function of the square root of the electric field normal to the RTIL/vacuum surface $\sqrt{|E_n|}$.

evaporation theory in eq 1 well in two regions (E_n < 1.4 V/nm and E_n > 1.8 V/nm). The fitted ϵ_r is 5.98 for E_n < 1.4 V/nm. A prior experiment reported that ϵ_r of the bulk [BMIM][PF_6] at 298.15 K is 11.4 ± 0.6.[32] The fitted value here is smaller mainly because it corresponds to the ϵ_r of the RTIL/vacuum surface, where the RTIL structure is different from that in the bulk. From liquid to vacuum, the RTIL density decreases (see Figure 4). With a smaller density at the RTIL/vacuum surface compared to that in the bulk, ions accommodate less to the external electric field; that is, the field is less screened, and the ϵ_r is smaller.[13] Another reason is that the temperature in our simulations is higher than that reported in the literature, and ϵ_r generally decreases as temperature increases.[33] For E_n > 1.8 V/nm, the fitted ϵ_r is 1.09. The difference in fitted ϵ_r between two regions implies that the RTIL/vacuum surface structure undergoes a transition as E_n increases from 1.4 to 1.8 V/nm. Because the intrinsic electric field in imidazolium-based RTILs is on the order of 1 V/nm, as E_n becomes stronger, the external field gradually overcomes the intrinsic field and alters the RTIL/vacuum surface structure: the ion density distribution across the surface becomes wider, and the magnitude of ion density becomes smaller.[34] As a result, the external field becomes further less screened at the RTIL/vacuum surface, and the ϵ_r decreases further. Apart from anion emission, cation emission is also simulated. When −1.8 < E_n < 0, cations rarely emit, and the associated j_e is nearly zero. When E_n < −1.8 V/nm, cation emission occurs, and Figure 2 shows that cation emission rates from simulations can also be fitted by eq 1. At the same $|E_n|$, the cation emission rate is observed to be smaller than anion emission rate. This is mainly because molecular structures of the cation and anion are different, and ΔG of the cation is larger than that of the anion, which makes the cation emission rate smaller (see eq 1).

In coarse-grained simulations, dimer emission is observed. However, the fraction of dimers is about 4% for different E_n, which differs from 20 to 40% reported in experiments for many different RTILs.[7,15,19] Although coarse-grained simulations can reproduce eq 1, they may miss atomistic details that play important roles in the composition of ion emission. To capture these details, we perform simulations with the united atom model, and fractions of dimers are found to be 22%, 26%, and 12% under fields of 1.3, 1.7, and 2.0 V/nm, respectively. In cases of 1.3 and 1.7 V/nm, simulation results agree with experimental data (20−40%),[7,15,19] suggesting that the united atom model can be used to study the composition of ion emission from RTILs. Considering the statistical error, the fractions of dimers in cases of 1.3 and 1.7 V/nm are nearly the same, while the fraction of dimers in the case of 2.0 V/nm is smaller. From 1.3 to 1.7 V/nm, the external field does not overcome the intrinsic electric field of the RTIL (united atom model), so the fraction of dimers remain almost unchanged. From 1.7 to 2.0 V/nm, the external field overcomes the intrinsic field, and it becomes easier to break the cation−anion pair, so the fraction of dimers decreases at 2.0 V/nm. Compared with available experimental data, the fraction of dimers at 2.0 V/nm in our simulations is smaller, which could be caused by the fact that RTILs and strengths of external electric fields in experiments are different from those in this work.[7,15,19]

Figure 3 shows typical snapshots of the RTIL/vacuum surface during monomer and dimer emissions. When anion

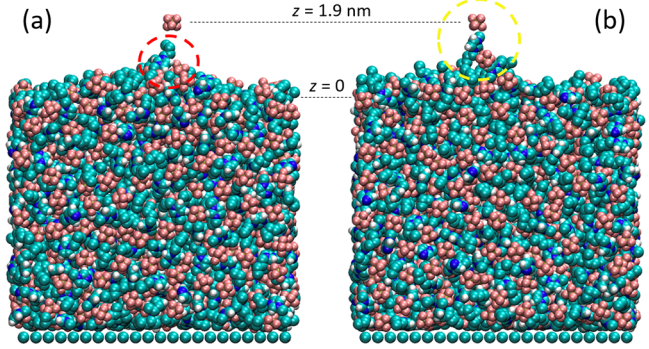

Figure 3. Snapshots of ion emission events from MD simulations with the united atom model: (a) a snapshot of monomer (PF_6^-) emission; (b) a snapshot of dimer ([BMIM][PF_6]PF_6^-) emission. Note that the anion is at z = 1.9 nm in both cases, and the z-direction is perpendicular to the electrode as shown in Figure 1a. z = 0 nm is the dividing surface position where the mass density of the RTIL is half of its bulk value.

emission occurs, a tip forms on the surface. A cation sits on top of the tip and is the closest to the emitted anion. For anion emission, the tip is usually composed of a cation and a few anions below it. In most cases, the emitting ion is connected to the tip until it reaches $z \approx$ 1.5 nm. As the emitting anion leaves the RTIL/vacuum surface, it will detach from the tip. However, the tip will not disappear immediately because of the long-range electrostatic interaction between the tip and the emitted ion. In Figure 3a, the emitted anion is at z = 1.9 nm, and we can still observe the tip. The tip will remain until the emitted anion moves further away from the RTIL/vacuum surface. It is also observed that the ring of the cation on the tip is always connected to anions below it. Because hydrogen atoms' charges on the cation's ring is relatively large, the strong electrostatic interaction between cation's ring and anions

https://dx.doi.org/10.1021/acs.jpclett.0c03335
J. Phys. Chem. Lett. 2021, 12, 711−716

below it makes it difficult for the cation to leave the RTIL/vacuum surface during anion emission.

Figure 3b shows a dimer emission event. The first emitted anion is at z = 1.9 nm. Unlike monomer emission, this anion still connects with the RTIL/vacuum surface through a finger. The anion is connected to the cation's ring, pulling the cation upward. The anion below the cation only has access to the cation's tail, and their interaction cannot provide a force as strong as the upward force on the cation from the first emitted anion. As a result, the cation starts to detach from the RTIL/vacuum surface. A cation−anion pair is difficult to be emitted because it is electrically neutral and the net force from the external field is zero. The pair needs to grab another ion so that the net charge of the emitted cluster is nonzero. Usually, the anion on the RTIL/vacuum surface closest to the cation's ring will be chosen, as the strong electrostatic interaction binds them together.

The formation of tips and fingers shows that the RTIL/vacuum surface is not flat, and the interfacial structure near the emitted ions is much richer than that modeled by ion evaporation theories. Consequently, the energy landscape calculations using these theories for ion emission from RTILs might not hold. Our results suggest that the structure of interfacial ions and interion interactions play important roles in the composition of ion emission. In general, cations and anions with stronger interion interactions would favor dimer emission, while the stronger interactions could suppress monomer emission. Therefore, at a certain E_n, RTILs with stronger interion interactions could exhibit a higher fraction of dimers than that of monomers.

Monomer emission provides a cleaner case to study underlying mechanisms. We focus on simulations with the united atom model under a field of 1.3 V/nm and analyze the RTIL density profile near the RTIL/vacuum surface and the emitting ion's trajectory. Figure 4 shows that the RTIL/vacuum surface spans from z = −0.5 nm to z = 0.7 nm. The emitting ion's trajectory shows that there exist two stages before anion emission. In the first stage, the emitting anion is below the surface (inset (a) of Figure 4). This is consistent with prior experimental and simulation results that anions stay underneath the RTIL/vacuum surface.[34] The anion is constrained by other cations at the surface; thus, it is in a relatively stable state, and ion emission cannot occur immediately. To be emitted, the anion has to first move to the top of the RTIL/vacuum surface: when t < 50 ps, the emitting anion stays around z = −0.1 nm; an abrupt displacement occurs at ∼50 ps, and the anion hops to z = 0.5 nm. On top of the RTIL/vacuum surface (inset (b) of Figure 4), the anion is at an activated state: its interactions with nearby cations become weaker, and it is ready to be emitted under the external field. The above analysis suggests that the anion needs to move across two barriers before emission: (1) move from a metastable state underneath the RTIL/vacuum surface to a metastable state on top of the surface; (2) detach from the RTIL/vacuum surface and move across the barrier above the surface.

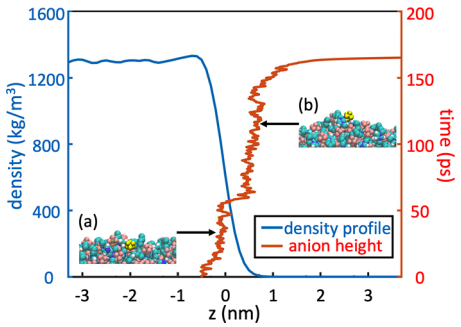

Figure 4. Mass density profile of RTILs along the z-direction (blue) and the evolution of coordinate in the z-direction as a function of time for the emitting anion (red). Insets: (a) a snapshot of the anion in the interior of the RTIL/vacuum surface; (b) a snapshot of the anion on top of the RTIL/vacuum surface.

Figure 5 shows temporal evolutions of coordinate, velocity, and force in the z-direction of an emitting anion. The anion

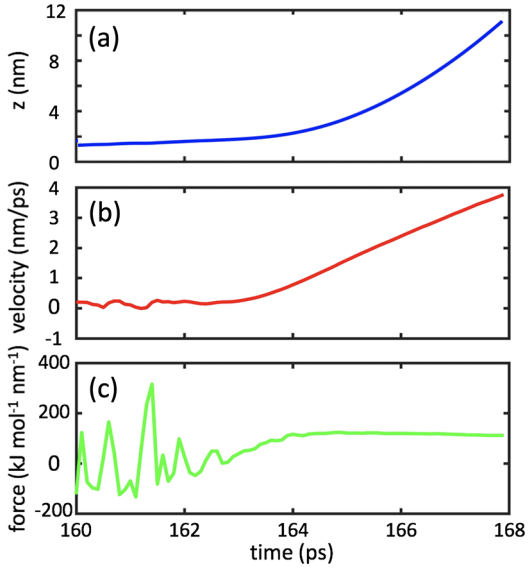

Figure 5. Coordinate (a), velocity (b), and force (c) in the z-direction of the emitting anion during its emission process.

starts to leave the RTIL/vacuum surface at ∼162.5 ps and escapes at ∼164 ps, during which it moves upward for ∼0.5 nm and its velocity is relatively small. After emission, the anion's coordinate and velocity in the z-direction increase significantly under the external field. When the anion is at the RTIL/vacuum surface, small displacements lead to relatively large fluctuations in force because of short-range interactions that are sensitive to interatomic distance. As the anion gradually leaves the RTIL/vacuum surface, the short-range interactions become weaker and the force's fluctuation becomes smaller. Before moving across the barrier above the surface, the anion is mainly subject to two forces: one from the external field pointing away from the RTIL/vacuum surface and the other one from the surface pointing toward the liquid. The first force is constant, while the second force generally decreases as the anion rises. The rising of the anion and the collapse of the tip (see Figure 3a) cause the second force to fluctuate, although the fluctuation's magnitude is smaller than that when the anion is below the RTIL/vacuum surface. In ion evaporation theories, the second force is due to the polarization of the RTIL/vacuum surface. Simulations here suggest that one needs to consider molecular details of ions and the fluctuating surface for ion emission from the RTIL/vacuum surface.

On the basis of the observation of tips and fingers on the RTIL/vacuum surface, we suppose that the different composition of ion emission is related to the different

https://dx.doi.org/10.1021/acs.jpclett.0c03335
J. Phys. Chem. Lett. 2021, 12, 711−716

metastable state of emitting ions near the surface. To sample the metastable states, we constrain one anion above the RTIL/vacuum surface at z = 1.9 nm and perform REMD simulations under a field of 0.9 V/nm. Other ions on the RTIL/vacuum surface cannot touch it by thermal fluctuation. The insets of Figure 6 show four identified metastable states: (a) a single anion detached from the surface, (b) a cation−anion pair detached from the surface, (c) a dimer detached from the surface, and (d) an anion connected to the surface through a finger. For each state, we calculate the probability distribution of the constraining force in the z-direction. Figure 6 shows that the probability distributions are different among different states. In state (a), the force is always negative, meaning that if an anion detaches from the RTIL/vacuum surface, a monomer emission will most likely occur. In state (b), the probability distribution varies in a wider range with a peak near 0 kJ/(mol nm), indicating that the anion could move either upward or downward. If the anion moves upward, the cation−anion pair will probably break by the external field as the neutral pair is difficult to emit, and a monomer emission occurs; if the anion moves downward, it is quite possible that the cation−anion pair will connect to the RTIL/vacuum surface. In state (c), the probability distribution also varies in a wide range with a peak near −180 kJ/(mol nm). Here the probability of sampling a negative force is higher, so the anion is more likely to move upward. Furthermore, the dimer has a nonzero net charge, and it feels an upward force from the external field; therefore, it is highly possible that a dimer emission will occur. In state (d), the probability distribution indicates that the anion could move either upward or downward. If it moves upward, emission may occur as monomer or dimer; if it moves downward, ions in the finger will probably return to the liquid. The above results show that the composition of ion emission depends on metastable states of the emitting ion near the RTIL/vacuum surface. These states are characterized by the emitting ion's different associations with nearby ions, which are further determined by molecular details of the ion/surface.

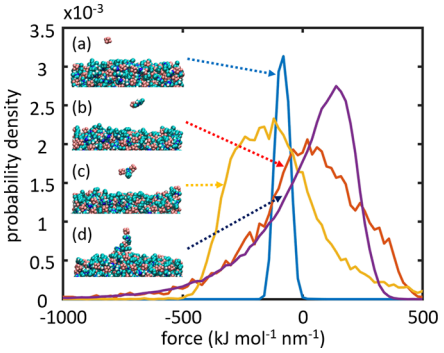

Figure 6. Probability distributions of the constraining force on the emitting anion for different metastable states from replica exchange molecular dynamics (REMD) simulations. The anion is constrained at z = 1.9 nm. Insets: (a) a single anion detached from the RTIL/vacuum surface; (b) a cation−anion pair detached from the RTIL/vacuum surface; (c) a dimer detached from the RTIL/vacuum surface; (d) the anion connected to the RTIL/vacuum surface through a finger.

In summary, we studied ion emission from the free surface of a planar RTIL film using MD simulations. The fact that eq 1 is recovered by simulations suggests that coarse-grained models can be used when large systems must be used, but only essential features of ion emission and RTILs must be captured, for example, in simulations of electrosprays from capillaries. By fitting eq 1 to MD data, we found that the fitted ϵ_r is smaller than that of the bulk RTILs, and its value varies in different regions of E_n, which was traced to the unique structure of the RTIL/vacuum surface and its variations under different external fields.

For monomer emission, we found that the emitting ion needs to move across two barriers before emission. The interaction between the emitting ion and the RTIL/vacuum surface was found to be more complex than that considered in ion evaporation theories. The fraction of dimers calculated by using the united atom model agrees with prior experimental data. We found that strong ion−ion interactions can lead to higher fraction of dimers in weaker external fields; in stronger fields, the fraction of dimers decreases because it becomes easier to break the cation−anion pair. REMD simulations were performed to identify metastable states of the emitting ion near the RTIL/vacuum surface. Results show that molecular details of the ion/surface determine the emitting ion's associations with nearby ions, which characterize its metastable states. These states strongly affect the composition of ion emission.

Insights from our work can help improve existing ion evaporation theories. For example, electric-field-dependent ϵ_r and the barrier for ion emission underneath the RTIL/vacuum surface could be incorporated into theories to better describe ion emission from RTIL/vacuum surfaces. The metastable state analysis proposed here for understanding ion emission compositions can be extended to obtain the free energy profile for ion emission. To do so, the ion needs to be constrained at various z-positions near the RTIL/vacuum surface, and the constraining forces from REMDs will be integrated along the z-direction to obtain an average free energy profile. Future work may also compare different force field models for RTILs in describing the rate and composition of ion emission. These analysis will form the theoretical basis for the rational selection of RTILs to achieve desired ion emission characteristics.

AUTHOR INFORMATION

Corresponding Author

Xikai Jiang − *State Key Laboratory of Nonlinear Mechanics, Institute of Mechanics, Chinese Academy of Sciences, Beijing 100190, China; School of Engineering Science, University of Chinese Academy of Sciences, Beijing 100049, China;* orcid.org/0000-0001-5601-8339; Email: xikaij@imech.ac.cn

Authors

Fei Zhang − *neoX Biotech, Beijing 102206, China*

Gaofeng Chen − *State Key Laboratory of Nonlinear Mechanics, Institute of Mechanics, Chinese Academy of Sciences, Beijing 100190, China; School of Engineering Science, University of Chinese Academy of Sciences, Beijing 100049, China*

Yadong He − *Department of Mechanical Engineering, Virginia Tech, Blacksburg, Virginia 24061, United States*

Guoqing Hu − *Department of Engineering Mechanics, State Key Laboratory of Fluid Power and Mechatronic Systems, Zhejiang University, Hangzhou, Zhejiang 310027, China*

Rui Qiao − *Department of Mechanical Engineering, Virginia Tech, Blacksburg, Virginia 24061, United States;* orcid.org/0000-0001-5219-5530

Complete contact information is available at:

https://dx.doi.org/10.1021/acs.jpclett.0c03335
J. Phys. Chem. Lett. 2021, 12, 711−716

https://pubs.acs.org/10.1021/acs.jpclett.0c03335

Notes

The authors declare no competing financial interest.

■ ACKNOWLEDGMENTS

The CAS Key Research Program of Frontier Sciences (QYZDB-SSW-JSC036) and the CAS Strategic Priority Research Program (XDB22040403) are acknowledged.

■ REFERENCES

(1) Luedtke, W. D.; Landman, U.; Chiu, Y.-H.; Levandier, D. J.; Dressler, R. A.; Sok, S.; Gordon, M. S. Nanojets, Electrospray, and Ion Field Evaporation: Molecular Dynamics Simulations and Laboratory Experiments. *J. Phys. Chem. A* **2008**, *112*, 9628−9649.
(2) de la Mora, J. F. The Fluid Dynamics of Taylor Cones. *Annu. Rev. Fluid Mech.* **2007**, *39*, 217−243.
(3) de la Mora, J. F.; Loscertales, I. G. The Current Emitted by Highly Conducting Taylor Cones. *J. Fluid Mech.* **1994**, *260*, 155−184.
(4) Fenn, J. B.; Mann, M.; Meng, C. K.; Wong, S. F.; Whitehouse, C. M. Electrospray Ionization for Mass Spectrometry of Large Biomolecules. *Science* **1989**, *246*, 64−71.
(5) Fenn, J. B.; Rosell, J.; Meng, C. K. Electrospray Ionization, How Much Pull does an Ion Need to Escape its Droplet Prison? *J. Am. Soc. Mass Spectrom.* **1997**, *8*, 1147−1157.
(6) Cole, R. B. *Electrospray and MALDI Mass Spectrometry: Fundamentals, Instrumentation, Practicalities, and Biological Applications*; John Wiley & Sons, Ltd.: Hoboken, NJ, 2010.
(7) Lozano, P.; Martínez-Sánchez, M. Ionic Liquid Ion Sources: Characterization of Externally Wetted Emitters. *J. Colloid Interface Sci.* **2005**, *282*, 415−421.
(8) Perel, J.; Mahoney, J. F.; Moore, R. D.; Yahiku, A. Y. Research and Development of a Charged-Particle Bipolar Thruster. *AIAA J.* **1969**, *7*, 507−511.
(9) Bischoff, L.; Mazarov, P.; Bruchhaus, L.; Gierak, J. Liquid Metal Alloy Ion Sources-An Alternative for Focussed Ion Beam Technology. *Appl. Phys. Rev.* **2016**, *3*, 021101.
(10) Romero-Sanz, I.; Bocanegra, R.; de la Mora, J. F.; Gamero-Castaño, M. Source of Heavy Molecular Ions based on Taylor Cones of Ionic Liquids Operating in the Pure Ion Evaporation Regime. *J. Appl. Phys.* **2003**, *94*, 3599−3605.
(11) Freemantle, M. *An Introduction to Ionic Liquids*; The Royal Society of Chemistry: London, 2009.
(12) Iribarne, J. V.; Thomson, B. A. On the Evaporation of Small Ions from Charged Droplets. *J. Chem. Phys.* **1976**, *64*, 2287−2294.
(13) Loscertales, I. G.; de la Mora, J. F. Experiments on the Kinetics of Field Evaporation of Small Ions from Droplets. *J. Chem. Phys.* **1995**, *103*, 5041−5060.
(14) Coffman, C. S.; Martínez-Sánchez, M.; Lozano, P. C. Electrohydrodynamics of an Ionic Liquid Meniscus during Evaporation of Ions in a Regime of High Electric Field. *Phys. Rev. E: Stat. Phys., Plasmas, Fluids, Relat. Interdiscip. Top.* **2019**, *99*, 063108.
(15) Larriba, C.; Castro, S.; de la Mora, J. F.; Lozano, P. Monoenergetic Source of Kilodalton Ions from Taylor Cones of Ionic Liquids. *J. Appl. Phys.* **2007**, *101*, 084303.
(16) Lozano, P.; Martínez-Sánchez, M. Ionic Liquid Ion Sources: Suppression of Electrochemical Reactions using Voltage Alternation. *J. Colloid Interface Sci.* **2004**, *280*, 149−154.
(17) Brikner, N.; Lozano, P. C. The Role of Upstream Distal Electrodes in Mitigating Electrochemical Degradation of Ionic Liquid Ion Sources. *Appl. Phys. Lett.* **2012**, *101*, 193504.
(18) Aarts, D. G. A. L.; Schmidt, M.; Lekkerkerker, H. N. W. Direct Visual Observation of Thermal Capillary Waves. *Science* **2004**, *304*, 847−850.
(19) Lozano, P. C. Energy Properties of an EMI-Im Ionic Liquid Ion Source. *J. Phys. D: Appl. Phys.* **2006**, *39*, 126−134.
(20) Borner, A.; Li, Z.; Levin, D. A. Prediction of Fundamental Properties of Ionic Liquid Electrospray Thrusters using Molecular Dynamics. *J. Phys. Chem. B* **2013**, *117*, 6768−6781.
(21) Prince, B. D.; Tiruppathi, P.; Bemish, R. J.; Chiu, Y.-H.; Maginn, E. J. Molecular Dynamics Simulations of 1-Ethyl-3-methylimidazolium Bis[(trifluoromethyl)sulfonyl]imide Clusters and Nanodrops. *J. Phys. Chem. A* **2015**, *119*, 352−368.
(22) Mehta, N. A.; Levin, D. A. Electrospray Molecular Dynamics Simulations using an Octree-based Coulomb Interaction Method. *Phys. Rev. E: Stat. Phys., Plasmas, Fluids, Relat. Interdiscip. Top.* **2019**, *99*, 033302.
(23) Higuera, F. J. Model of the Meniscus of an Ionic-Liquid Ion Source. *Phys. Rev. E* **2008**, *77*, 026308.
(24) Micaelo, N. M.; Baptista, A. M.; Soares, C. M. Parametrization of 1-Butyl-3-methylimidazolium Hexafluorophosphate/Nitrate Ionic Liquid for the GROMOS Force Field. *J. Phys. Chem. B* **2006**, *110*, 14444−14451.
(25) Roy, D.; Maroncelli, M. An Improved Four-Site Ionic Liquid Model. *J. Phys. Chem. B* **2010**, *114*, 12629−12631.
(26) Raghunathan, A. V.; Aluru, N. R. Self-Consistent Molecular Dynamics Formulation for Electric-Field-Mediated Electrolyte Transport through Nanochannels. *Phys. Rev. E* **2007**, *76*, 011202.
(27) Hess, B.; Kutzner, C.; van der Spoel, D.; Lindahl, E. GROMACS 4: Algorithms for Highly Efficient, Load-Balanced, and Scalable Molecular Simulation. *J. Chem. Theory Comput.* **2008**, *4*, 435−447.
(28) Wu, P.; Huang, J.; Meunier, V.; Sumpter, B. G.; Qiao, R. Voltage Dependent Charge Storage Modes and Capacity in Subnanometer Pores. *J. Phys. Chem. Lett.* **2012**, *3*, 1732−1737.
(29) Martínez, L.; Andrade, R.; Birgin, E. G.; Martínez, J. M. PACKMOL: A Package for Building Initial Configurations for Molecular Dynamics Simulations. *J. Comput. Chem.* **2009**, *30*, 2157−2164.
(30) Sachs, J. N.; Crozier, P. S.; Woolf, T. B. Atomistic Simulations of Biologically Realistic Transmembrane Potential Gradients. *J. Chem. Phys.* **2004**, *121*, 10847−10851.
(31) Sugita, Y.; Okamoto, Y. Replica-Exchange Molecular Dynamics Method for Protein Folding. *Chem. Phys. Lett.* **1999**, *314*, 141−151.
(32) Wakai, C.; Oleinikova, A.; Ott, M.; Weingärtner, H. How Polar Are Ionic Liquids? Determination of the Static Dielectric Constant of an Imidazolium-based Ionic Liquid by Microwave Dielectric Spectroscopy. *J. Phys. Chem. B* **2005**, *109*, 17028−17030.
(33) Hunger, J.; Stoppa, A.; Schrödle, S.; Hefter, G.; Buchner, R. Temperature Dependence of the Dielectric Properties and Dynamics of Ionic Liquids. *ChemPhysChem* **2009**, *10*, 723−733.
(34) Shi, R.; Wang, Y. Surface Structure of Ionic Liquids under an External Electric Field. *Mol. Simul.* **2017**, *43*, 1295−1299.